Enhancing Laser-Driven Ion Acceleration through Computational Methods

DISSERTATION

Presented in Partial Fulfillment of the Requirements for the Degree Doctor of Philosophy in the Graduate School of The Ohio State University

By

Ronak Desai, B.S., M.S.

Graduate Program in Physics

The Ohio State University

August 2025

Dissertation Committee:

Professor Chris Orban, Advisor

Professor Douglass Schumacher

Professor Alexandra Landsman

Professor Brian Skinner

Abstract

An abstract goes here. It should be less than **500 words**.

To you, my love.

Acknowledgments

I want to thank your mom...

Vita

May, 2019	B.S. Physics, B.A. Mathematics, Rowan University, Glassboro, NJ
August 2020 - July 2021	Graduate Fellow, The Ohio State University, Columbus, OH
August 2021 - April 2023	Graduate Teaching Associate, The Ohio State University, Columbus, OH
August, 2023	M.S. Physics, The Ohio State University, Columbus, OH
August 2023 - July 2025	Graduate Research Associate, The Ohio State University, Columbus, OH

Publications

Applying Machine Learning Methods to Laser Acceleration of Protons: Lessons Learned from Synthetic Data

Towards Automated Learning with Ultra-Intense Laser Systems Operating in the kHz Repetition Rate Regime

Intelligent Control of MeV Electrons and Protons

Can Two Pulses Enhance Proton and Electron Acceleration?

Fields of Study

Major Field: Physics

Table of Contents

List of Figures

Figure **Page**

List of Tables

Table **Page**

Chapter 1
Laser-Plasma Interactions and Ion-Acceleration

1.1 Plasma Physics

Chen[9] describes a plasma as

> a *quasineutral* gas of charged and neutral particles which exhibits *collective behavior*

In this section, the quasineutrality and collective behavior of plasmas will be discussed. One way to create a plasma is through the interaction of matter with an energetic laser. The laser has enough energy to ionize atoms to a hot dense soup that satisfy the definition of Chen. Plasmas do exist in other contexts, like those found in stars and various astrophysical systems, but these will not be explained in detail in this section. Here, we'll overview the physics of gaussian laser beams, particle motions in electric fields, and the properties of plasmas.

1.1.1 Gaussian Laser

In order to heat up a material with a laser efficiently, the energy would ideally be concentrated to a small point. For example, the typical incandescent household light bulb radiates energy equally in all directions and does not do a good job of focusing energy to a point. But, using a magnifying glass can effectively concentrate the energy. For this reason, focusing optics play an important part in the field of plasma physics.

However, to obtain a focused light source, we can use lasers that have the capability of producing narrow beams. The intended output of many lasers have an electric field described by the fundantal transverse electromagnetic mode[10] (TEM_{00}) described by the following electric field

$$E(r,x) = E_0\hat{y}\frac{w_0}{w(x)}\exp(-\frac{r^2}{w(x)^2})\cos(kx - \arctan(x/x_R) + \frac{kr^2}{2R(x)}) \tag{1.1}$$

where $\hat{x}$ is the propagation direction, $\hat{y}$ is the polarization direction, and $r = \sqrt{y^2 + z^2}$ is the radial distance away from the laser axis. In the cosine function, $R(z) = z[1 + (z_R/z)^2]$ is the radius of curvature and $\arctan(z/z_R)$ is the guoy phase. For our purposes, these won't have too much relevance. Additionally, the beam radius w is expressed as

$$w(z) = w_0\sqrt{1 + (z/z_R)^2} \tag{1.2}$$

and has a minimum value at the *beam waist* $w(0) \equiv w_0$ at the focal position of the laser. The length scale over which the beam can propagate without diverging significantly is the *Rayleigh range* $x_R \equiv \frac{\pi w_0^2}{\lambda}$. The peak intensity is related to the electric field by $I_0 = \frac{1}{2}\epsilon_0 c E_0^2$ and eq. (1.1) shows that the intensity decays as $I(x, r) = I_0(w_0/w(x))^2 \exp(-2r^2/w(x)^2)$ with increasing r and x. If we integrate this intensity distribution over the entire $y - z$ plane, we obtain the peak power $P_0 = \frac{\pi\omega_0^2}{2} I_0$. Furthermore, we can integrate the power over the pulse duration (assuming the pulse has a $sin^2(t)$ envelope) to obtain the total energy in the pulse

$$E = \frac{\pi\omega_0^2}{2} I_0 \tau_{\text{fwhm}} \tag{1.3}$$

where τ_{fwhm} is the full-width half-max and is equal to half the pulse duration for a $sin^2(t)$ pulse envelope.

1.1.2 Single Particle Motions

Electrostatics is governed by the Maxwell's equations which describe the allowed wave-like solutions for electric and magnetic fields in both matter and vacuum. The most relevant equation in this section is Gauss' Law or Poisson's Equation which can be expressed as

$$-\nabla^2\phi = \nabla \cdot \vec{E} \equiv \frac{\rho}{\epsilon_0} \tag{1.4}$$

which relates the electrostatic potential ϕ or electric field E to the charge density ρ. This equation highlights how electric fields are directed radially outward from positive charges and inward towards negative charges. The motion of an electron in the influence of an electric field E or magnetic field B is given by the *Lorentz force* F_L

$$F_L \equiv -e(\vec{E} + \vec{v} \times \vec{B}) \tag{1.5}$$

Quiver Energy

To gain intuition about some quantities of interest for laser-matter interactions, let's consider a simple problem of an electron of charge $-e$ governed by eq. (1.5) with a negligible magnetic field B. Additionally, only consider 1D motion in the oscillating field

$E = E_0 \cos(\omega t)$ for a laser field of frequency ω. Then, the equation of motion is

$$\frac{dv}{dt} = -\frac{eE_0}{m}\cos(\omega t) \tag{1.6}$$

We can integrate this equation to obtain the velocity and position as a function of time (assuming $x_0 = v_0 = 0$)

$$v(t) = -v_{\text{osc}}\sin(\omega t) \tag{1.7}$$

$$x(t) = \frac{v_{\text{osc}}}{\omega}[\cos(\omega t) - 1] \tag{1.8}$$

where $v_{\text{osc}} \equiv (eE_0)/(m\omega)$ is defined as the *quiver velocity*. From Equation 1.7, we can calculate the kinetic energy gained by an electron as $U_p \equiv \frac{1}{2}m\langle v^2\rangle = \frac{1}{4}mv_{\text{osc}}^2$ which is known as the *ponderomotive potential (energy)*. This energy represents the cycle-averaged quiver energy of an electron in an electromagnetic field. A more common term used is the *normalized vector potential* a_0 which is closely related to the quiver velocity

$$a_0 \equiv v_{\text{osc}}/c = \frac{eE_0}{m\omega c} \tag{1.9}$$

Ultra-intense laser-matter interactions involve relativistic electrons which are produced when $a_0 \gtrsim 1$. In terms of the field, $a_0 \sim 1$ corresponds to a peak electric field $E_0 = \frac{2\pi mc^2}{e\lambda} \simeq 4\,\text{TV}\,\text{m}^{-1}$. A more common expression of the field strength is given by the peak intensity, which can be calculated as $I_0 = \frac{1}{2}c\epsilon_0 E_0^2 \simeq 2\times10^{18}\,\text{W}\,\text{cm}^{-2}$ for this electric field. Consequently, the threshold for relativistic interactions is commonly understood as $I_0 \gtrsim 1\times10^{18}\,\text{W}\,\text{cm}^{-2}$.

Ponderomotive Force

The above approach yields some important scales for laser-matter interactions, but only describes the interaction of a plane wave that is spatially homogeneous. A real laser field would be spatially inhomogeneous and we can express $E(x) \approx E_0 + xE_0'(x)$ to first order. This modifies the equation of motion as

$$\frac{dv}{dt} = -\frac{eE_0}{m}\cos(\omega t) - \frac{eE_0'}{m}\cos(\omega t)[\frac{v_{\text{osc}}}{\omega}(\cos(\omega t) - 1)] \tag{1.10}$$

where we've inserted the expression for x from eq. (1.8) which should be approximately true for small x. This equation can be simplified and separated into oscillating and non-oscillating components (cite arefiv notes) as

$$\frac{dv}{dt} = -\frac{eE_0}{m}[\cos(\omega t)(1 - \frac{E_0'v_{\text{osc}}}{e_0\omega}) + \frac{E_0'v_{\text{osc}}}{2\omega E_0}\cos(2\omega t)] - \frac{eE_0'v_{\text{osc}}}{2m\omega} \tag{1.11}$$

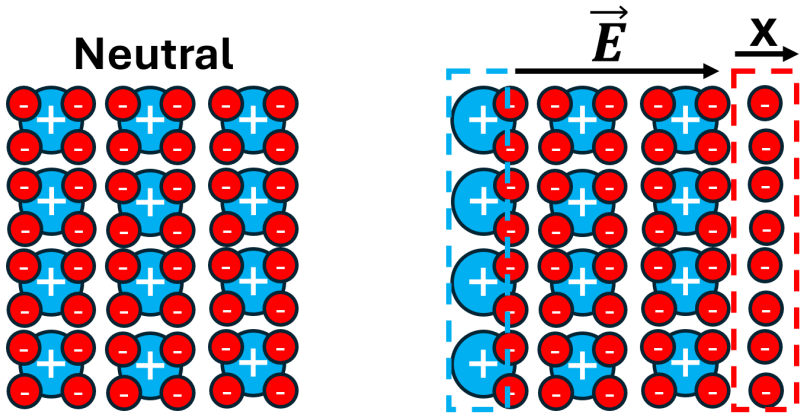

Figure 1.1: An initially charge-neutral plasma is depicted on the left. On the right, the electrons are displaced by a distance x creating a charge separation and electric field akin to a parallel-plate capacitor directed towards the right. Adapted from Smith[1].

Over many cycles, the oscillating components will average out to zero and the remaining term is given by $\langle F_p \rangle = m\frac{dv}{dt} = -\frac{eE_0' v_{\text{osc}}}{2m\omega}$ and is called the *ponderomotive force*. We can generalize this to 3D and express this time-averaged force in several different, equivalent ways

$$\langle F_p \rangle = -\frac{e^2}{2m\omega^2}|E_0|\nabla E_0 = -\frac{mc^2}{4}\nabla(a_0^2) = -\nabla U_p \tag{1.12}$$

where

$$U_p = \frac{e^2 E_0^2}{4m\omega^2} = \frac{1}{4}mv_{\text{osc}}^2 \tag{1.13}$$

is the ponderomotive potential energy introduced earlier.

The ponderomotive force is an important mechanism in the absorption of laser energy by electrons which will be expanded upon (LATER: CITE SECTION).

1.1.3 Properties of a Plasma

The quasi-neutrality condition reflects the fact that a plasma is charge neutral throughout its volume in a similar way to an ideal conductor: mobile electrons will reorganize themselves in the presence of an external electric field to maintain zero field (or constant potential). The simplest plasma description will assume the ions are immobile (due to being much heavier than the electrons) and can be treated as a constant neutralizing background density n_i for the electrons of density $n_{e,0} = Zn_i$ (for a plasma with atomic number Z).

Plasma Electron Oscillations

A simple example can be illustrated by fig. 1.1 which shows a sheet of negative charge density $-\sigma = -en_e x$ displaced to the right a small distance x. The region in the bulk of the plasma will experience a force from the parallel plate "capacitor" fields directed to the right.

$$F = m\frac{d^2x}{dt^2} = -e\frac{en_e x}{\epsilon_0} \tag{1.14}$$

which has the form of a restoring force that brings the charge imbalance back to the center of the plasma. This oscillatory motion has an associated frequency

$$\omega_{p,e} = \sqrt{\frac{n_e e^2}{m_e \epsilon_0}} \tag{1.15}$$

that gives the timescale for electron motion in the plasma. This characteristic frequency shows why plasmas support collective motion (in opposition to a neutral gas in which collisions between individual particles only happen). To get a feeling for this timescale, let's assume a somewhat typical electron density $1 \times 10^{29}\,\mathrm{m}^{-3}$ in laser-plasma interactions to yield a timescale of $\omega_{p,e}^{-1} \simeq 0.1\,\mathrm{fs}$.

Naturally (without externally imposed forces), these fluctuations in charge would be caused by thermal motions of electrons with a characteristic speed v_{th}

$$v_{th} = \sqrt{\frac{k_B T_e}{m}} \tag{1.16}$$

Due to the strong restoring force from the charge separation, the electrons can only move a short distance λ_D, called the Debye length, out of equilibrium in this timescale. We can estimate this length by equating $v_{th} = \lambda_D/t \simeq \lambda_D \omega_{p,e}$ and solve for λ_D.

$$\lambda_D = \frac{v_{th}}{\omega_{p,e}} = \sqrt{\frac{\epsilon_0 k_B T_e}{n_e e^2}} \tag{1.17}$$

Physically, λ_D gives a length scale over which the electrostatic force persists in a plasma. Within a distance λ_D from some perturbation, charges will feel a force, and outside this distance, the charges will be completely shielded like that of an ideal conductor.

Fluid Model

This description of a plasma as a sea of electrons with collective motion and an oscillatory wave-like nature naturally lends itself toward a fluid model. The first component of this model stems from eq. (1.5) whose explicit time and space dependence can be expressed through $\frac{dp}{dt} = m(\frac{\partial v}{\partial x}\frac{\partial x}{\partial t} + \frac{\partial v}{\partial t}) = m(\frac{\partial v}{\partial t} + v\frac{\partial v}{\partial x})$ (just considering one spatial dimension for

simplicity). The second component of this model is the effect of the pressure gradient from thermal motions. Particles will tend to migrate from areas of higher pressure to lower pressure, where the thermal pressure is typically given by the familiar ideal gas law equation of state $p = n_e k_B T_e$. Consequently, the equation of motion should have a term that is opposite to the pressure gradient direction (i.e. $-\nabla p$). Combining these two components together in a generalized 3D equation results in

$$mn_e(\frac{\partial \vec{u}}{\partial t} + (\vec{u}\cdot\nabla)\vec{u}) = -en_e(\vec{E} + \vec{u}\times\vec{B}) - \nabla p \tag{1.18}$$

where we've changed the single particle velocity $\vec{v}$ to the fluid velocity $\vec{u}$ and multiplied by the electron density n_e to ensure correct units with the pressure gradient term. Then, let's look for a simple radially symmetric solution where the fluid velocity $u = 0$, magnetic field B is negligible, and the temperature is constant (isothermal). Then,

$$n_e eE = -k_B T_e \frac{\partial n_e}{\partial r} \tag{1.19}$$

and by relating the electric field to the potential $E = -\frac{dV}{dx}$, this equation can be integrated from $n_{e,0} \to n_e$ and $0 \to \phi$ to obtain

$$n_e = n_{e,0}\exp(\frac{e\phi}{k_B T_e}) \tag{1.20}$$

which is referred to as the *Boltzmann relation* for electrons[9]. We can get an approximate solution to this equation when the potential ϕ is only slightly larger than the equilibrium $\phi = 0$, which can be found when $e\phi << k_B T_e$. We can Taylor expand the density to obtain

$$n_e \approx n_{e,0}(1 + \frac{e\phi}{k_B T_e}) \tag{1.21}$$

and if we assume a fully ionized plasma with immobile ions of charge Z, the density of ions satisfies $ne, 0 = Zn_i$ and eq. (1.4) becomes

$$\epsilon_0\nabla^2\phi = -en_{e,0} + en_e = en_{e,0}[1 + \frac{e\phi}{k_B T_e} - 1] = \frac{e^2 n_{e,0}\phi}{k_B T_e} \tag{1.22}$$

This equation admits solutions of an exponentially decaying potential

$$\phi(r) = \frac{Q}{r}\exp(-\frac{r}{\lambda_D}) \tag{1.23}$$

where $\lambda_D = \sqrt{\frac{\epsilon_0 k_B T_e}{n_{e,0}e^2}}$ is the Debye length from eq. (1.17). A visualization of the decaying potential from eq. (1.23) is shown in fig. 1.2. Looking at the center panel, we can see the fields drop off quickly within a distance λ_D in contrast to the left panel's potential that extends much further out in distance r. The exponentially decaying potential is a feature of plasmas and highlights the ability of plasma electrons to shield fields in a distance λ_D.

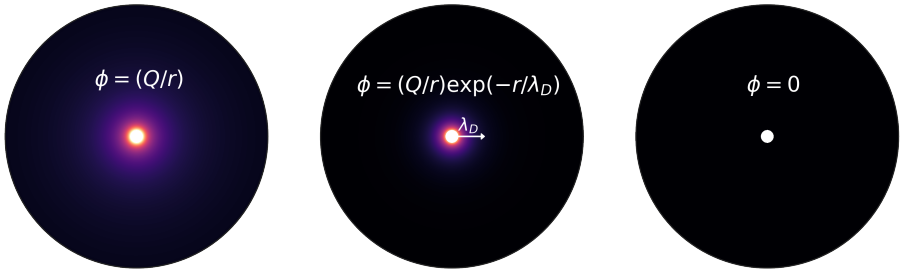

Figure 1.2: Visualization of the electric potential as a function of radial distance away from a positive point charge at the origin in three scenarios: vacuum (left), plasma (center), ideal conductor (right). Brighter colors show a higher value of ϕ. In the center panel, the debye length λ_D is shown.

Plasma Conditions

Putting all this together, we can define several conditions that must be satisfied for a plasma[9]. Quasi-neutrality dictates that the plasma should be largely charge neutral. The only regions that aren't charge neutral are those that fall within λ_D of some charge imbalance. Therefore, if L is the length scale of the system in which the plasma resides, we require that $\lambda_D \ll L$. However, this condition is not sufficient because an ideal conductor has $\lambda_D = 0$ but is not a plasma due to the absence of collective behavior. Collective behavior can be enforced by asserting that there are enough electrons N_D within a spherical volume of radius λ_D. The corresponding equation is $N_D = n_e(\frac{4}{3}\pi\lambda_D^3) \gg 1$. The final condition is that electrostatic interactions should dominate over collisions because the collective behavior (e.g. plasma oscillations) originates from the electrostatic forces. This means that the period of oscillations ($\omega_{p,e}^{-1}$) should be less than the mean time between collisions.

the cor For example, consider the problem of adding a point charge Q at the origin of Resonant Absorption, Brunel (Not so resonant, resonant absorption), and JxB Heating.

Wilks [2] uses PIC simulations to find that hot electron temperature is approximately equal to ponderomotive electron energy gained in oscillating electric field. Compares this to laser accelerating electron in thin layer of skin depth on the surface.

Brunel [5] descibes "not so resonant, resonant absorption"

1.1.4 Absorption of Energy

In order for a laser to couple energy to the plasma electrons, some absorption mechanism needs to take place. The most obvious way that electrons can gain energy is through collisions with other energetic electrons and ions. However, the collision frequency is known

to get smaller as the temperature goes up[6], so much so that plasmas can be treated as collisionless for ultra-intense laser experiments. Below, some of the most common known heating mechanisms are summarized.

Critical Density

First, we will look at how the electric field from an oscillating electric field penetrates a plasma. Using **????** combined with the vector identity $\nabla \times (\nabla \times \vec{E}) = \nabla(\nabla \cdot \vec{E}) - \nabla^2 \vec{E}$[10], we can solve for the vector wave equation in terms of only $\vec{E}$.

$$(\nabla^2 - \frac{1}{c^2}\frac{\partial^2}{\partial t^2})\vec{E} = \mu_0 \frac{\partial J}{\partial t} + \nabla(\nabla \cdot \vec{E}) \tag{1.24}$$

We can look for solutions of $\vec{E} = E(x)\cos(\omega t)\hat{x}$ that vary spatially only in the x direction. We are assuming $E(0)$ is the amplitude of the electric field at the boundary between vacuum $x < 0$ and matter $x > 0$ and wish to understand the form of $E(x)$ when $x > 0$. To proceed, we can assume the current density can be related to the drift velocity[11] by $J = -n_e e u$ where u is the electron fluid velocity that satisfies eq. (1.18). Ignoring B and thermal pressure, this relationship becomes

$$\frac{\partial \vec{J}}{\partial t} = \frac{n_e e^2}{m} E = \omega_p^2 \epsilon_0 \vec{E} \tag{1.25}$$

using eq. (1.15) which can be combined with the vector wave equation to obtain a differential equation for the electric field

$$[\nabla^2 + \frac{\omega^2}{c^2}(1 - \frac{\omega_p^2}{\omega^2})]\vec{E} = 0 \tag{1.26}$$

By just focusing on the x-dependence, we can simplify this equation to

$$\frac{d^2 E}{dx^2} = \frac{1}{l_s^2} E \tag{1.27}$$

where $l_s^2 \equiv \frac{c^2}{\omega^2 - \omega_p^2}$ defines the *skin depth* l_s. In the case where $\omega < \omega_p$, l_s^2 is negative and the solution has a sinusoidal dependence

$$E(x) = E(0)\cos(x/l_s) \tag{1.28}$$

On the other hand, when $\omega > \omega_p$, l_s^2 is positive and the solution has an exponential dependence

$$E(x) = E(0)\exp(-x/l_s) \tag{1.29}$$

where $l_s \equiv c/\omega_p$ is defined as the *skin depth*. This "evanescent" behavior when $\omega > \omega_p$ occurs because the electrons cannot respond fast enough to the higher frequency ω. Since the field cannot propagate effectively for $x > 0$, the plasma ends up reflecting a significant portion of the light. Since wavelength (and frequency) is fixed from the laser, we can reformulate this finding in terms of electron density. The critical density n_c is defined as the electron density where $\omega = \omega_{p,e}$. Using eq. (1.15), this can be expressed as

$$n_c \equiv \frac{m\epsilon_0}{e^2}\omega^2 \tag{1.30}$$

When $n_e > n_c$, the plasma is said to be *overdense* and most of the laser light gets reflected. When $n_e < n_c$, the plasma is said to be *underdense*, and the laser light can propagate through the plasma.

A typical Ti:Sapphire laser has a wavelength of 0.8 µm which corresponds to a critical density of $n_c \simeq 1.7 \times 10^{27}\,\mathrm{m}^{-3}$. In this work, two materials are of interest: gold and ethylene glycol which have densities of $19.3\,\mathrm{g\,cm}^{-3}$ and $1.11\,\mathrm{g\,cm}^{-3}$ respectively. These mass densities correspond to a number density of electrons $5.9 \times 10^{28}\,\mathrm{m}^{-3}$ and $1.1 \times 10^{28}\,\mathrm{m}^{-3}$ respectively assuming a singly ionized plasma. If the plasmas were multiply ionized, these densities would be even higher. Even though these "solid density" plasmas are clearly overdense, experiments show energy is able to efficiently couple to the electrons. Consequently, there must exist mechanisms of absorption that are consistent with the fact that most of the laser energy can only be deposited in a small depth l_s into the plasma.

Resonance Absorption

The previous discussion applied to an electric field directed in the x-direction. For gaussian laser beams, the electric field is always perpendicular to the direction of propagation. So, if the laser beam is to be directed toward a target at $x = 0$, normal incidence would imply that the electric field $E_x = 0$. Additionally, an s-polarized beam would have an electric field only in the z direction. As a result, the typical model of a laser beam depositing energy into a plasma involves a p-polarized laser beam traveling obliquely in the $x - y$ plane with some angle of incidence θ_i measured with respect to the normal direction of the target. Physically, plasma oscillations occur through fluctuations in density which are going to be the strongest in the x direction due to the interface between vacuum and matter.

Furthermore, Kruer[12] argues that the reflection of light at oblique incidence occurs at a density $n_e = n_c \cos^2(\theta_i)$ by enforcing momentum conservation of the electric field component in the y direction. Even though we've discussed density profile as an abrupt step: from 0 to n_e from crossing $x = 0$, an actual experiment would see some pre-heating of the target before the target becomes ionized and behaves as a mirror at the critical density. This can be characterized by some scale length $L_p \equiv n_e(\frac{\partial n_e}{\partial x})^{-1}$ which is smaller for steeper density

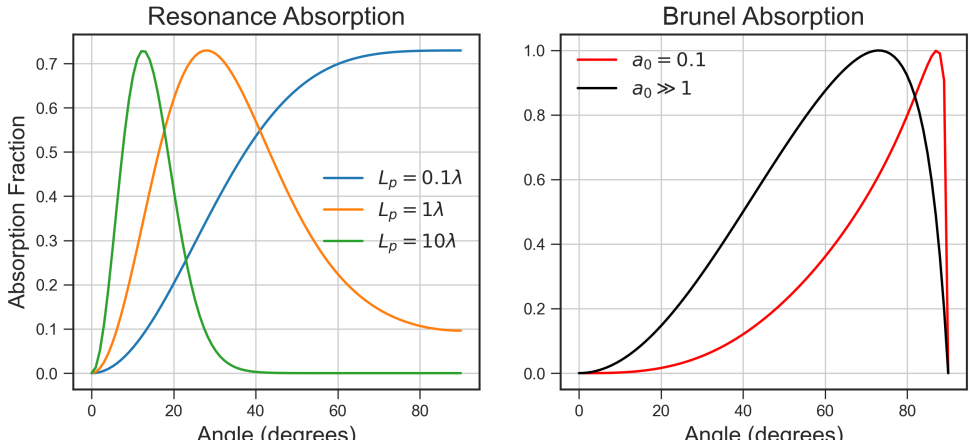

Figure 1.3: Absorption fraction as a function of incidence angle θ_i. For resonance absorption, the density scale length L_p is varied in terms of the laser wavelength $\lambda = 0.8\,\mu$m. For the Brunel mechanism, fractions are plotted for two regimes $a_0 \ll 1$ (where a value of $a_0 = 0.1$ was chosen) and for $a_0 \gg 1$ (which has no dependence on a_0).

profiles. As a result, at higher incidence angles, the evanescent portion of the electric field has to travel further into the underdense region of the target to reach the critical density.

When the frequency of the laser $\omega \simeq \omega_p$, the laser light is in resonance with the plasma oscillations and the energy can be most efficiently absorbed. To maximize the amount of energy reaching the critical density surface in resonance, we would want θ_i to be large so that the electric field has a significant component in the x direction, but also small enough so that the field doesn't diminish too much by traveling in the evanescent underdense region. Denisov[13] and others[14–16] addresses this question and develops a model for this so-called *resonance absorption* An approximate version of this formula is given by Kruer[12]

$$\phi(\tau) \simeq 2.3\tau \exp(-2\tau^3/3) \tag{1.31}$$

where $\tau \equiv (kL_p)^{1/3} \sin(\theta_i)$ takes into account both the scale length and incidence angle. fig. 1.3 shows the fractional absorption $\phi(\tau)^2/2$ of the incident light from this model as a function of θ_i for various scale lengths.There is an optimal angle $\theta_{max} \approx \arcsin(0.8(kL_p)^{-1/3})$ that maximizes the absorption fraction (although Kruer notes that his simple model overestimates the peak absorption – the fraction should peak at around 0.5[12]).

Brunel Heating

Resonance absorption only makes sense when the amplitude of the plasma oscillations $x_{\text{osc}} = v_{\text{osc}}/\omega = \frac{a_0\lambda}{2\pi}$ is less than the scale length L_p[6], otherwise there is not enough available space for the oscillations to take place. For $\lambda = 0.8\,\mu$m and $a_0 = 1$, $x_{\text{osc}} = 127\,$nm. However, for

extremely small scale-lengths, efficient electron heating can still be observed (SOURCES OF EXPERIMENTS). Consequently, a different type of heating mechanism is responsible in this case (somewhat confusingly) called "not so resonant, resonant absorption"[5]. This model, developed by Brunel, is also known as *Brunel heating* and will be explained below.

Before explaining the Brunel mechanism, I should the basics of the 3-step model used for high-harmonic generation[17]. Readers may find this model more familiar due to the recent 2023 Nobel Physics Prize won by Ohio State's Pierre Agostini[18] which utilized the ideas of this model to produce attosecond pulses. This model involves a strong oscillating electric field $E(x) = E_0 \cos(\omega t)$ incident on an atom. Now, assume an electron is ionized at $t = t*$. Under the influence of the oscillating field, the (initially stationary) electron will gain and lose energy by moving away from the atom and returning back toward the atom. When $t \neq t*$, it is actually possible for the electron to return back to the atom with non-zero energy. In fact, when $\omega t^* \approx 17° + n(180°)$ for integer n, the electron returns with an energy peaking at $3.17U_p$ where U_p is the ponderomotive potential given by eq. (1.13). Furthermore, modeling the ionization rate through quantum-mechanical tunneling of an electron through a Coulomb potential warped by the oscillating laser field, we also determine that the most probable energy for an electron is strongly peaked at the $3.17U_p$ cutoff. In short, this model shows how a laser field can produce electrons with energy on the scale of the ponderomotive potential with high probability at a frequency of twice per optical cycle.

In the Brunel mechanism[5], we are considering a laser field incident on a planar target at $x > 0$ and vacuum at $x < 0$. In order for the electrons to escape the target, there needs to be some component of the electric field in the x direction. Thus, we need to consider oblique incidence and p-polarization just like with resonance absorption. When the plasma scale length is small, the electrons will be able to travel far enough in the $x < 0$ to escape the plasma entirely and gain energy on the order of U_p in a similar fashion to Corkum's model[17]. Electrons arriving back to the target at just the right time will penetrate deeper than the skin depth $l_s \approx c/\omega_p$ and be inaccessible to the laser field[6]. These *hot electrons*, generated primarily on the front surface of the target, will provide the energy to heat the remainder of the overdense region of the target that the laser field cannot directly access.

As mentioned, the optimal angle would appear to be for grazing incidence ($\theta_i = 90°$), but Gibbon notes that accounting for imperfect reflection of the laser field and relativistic energies of the electrons, the efficiency no longer diverges at $\theta = 90°$[6]. In fig. 1.3, some estimates for the absorption efficiency are plotted according to a simplified model developed by [6] based on Brunel[5].

Other Mechanisms

When the laser field penetrates a distance $l_s \approx c/\omega_p$ into the overdense region of the target, the electrons can heat up through collisions at an absorption rate $\eta \propto \frac{\nu_{ei}}{\omega_p, i}$[6] where ν_{ei} is

the electron-ion collision frequency. This type of absorption is called the *skin effect*. In this case, we see Fresnel-like reflection and absorption (see[19]) that is effective for large incidence angles. Even when the collision frequency is low, we can still get efficient absorption as long as the thermal electron motions are large compared to the skin depth (i.e. $v_{th}/\omega > l_s$)[6]. This phenomena is called the *anomalous skin effect* that is also most effective at large incidence angles.

All of the mentioned phenomena work best at oblique incidence in p-polarization. But, for relativistic intensities, additional heating mechanisms arise. When $a_0 \gtrapprox 1$, the magnetic portion of eq. (1.5) becomes significant. At normal incidence, the electric and magnetic field components both fall in the $y-z$ plane. The electric fields move the electrons strongly causing a current $\vec{J}$ which in turn will interact with the laser magnetic field $\vec{B}$ in the direction perpendicular to both. As a result, this type of heating is known as $\vec{J}\times\vec{B}$ heating[6, 20]. Because $\vec{J}\times\vec{B}$ is in the direction of propagation, this effect is most pronounced at normal incidence.

At even higher intensities, the laser can directly impart energy to the electrons through radiation pressure[21] because photons themselves carry momentum. These mechanisms are explored further in section 1.2. In reality, all experiments involve a combination of several different electron heating mechanisms. Consequently, many experiments and simulations have been devoted to parametric studies that show how parameters (L_p, θ_i, polarization, a_0, etc.) affect electron absorption

1.2 Ion Acceleration

The previous section gave an overview of the laser-plasma interactions and how they can efficiently couple energy into hot electrons. Regardless of heating mechanism, one theme is common to all – the energy gained by an electron's quiver motion in an oscillatory field, known as the ponderomotive potential (eq. (1.13)) sets the scale for the hot electron temperature T_h. That equation was only valid for non-relativistic electrons, so we must replace $U_p = \frac{1}{4}mv_{\text{osc}}^2$ with the relativistic kinetic energy $U_p \equiv (\gamma-1)mc^2$ where $\gamma = 1/\sqrt{1-\frac{v_{\text{osc}}^2}{c^2}}$ defines the lorentz factor. We can combine this with the relativistic momentum $p=\gamma m v_{\text{osc}}$ and eq. (1.9) to determine an approximate expression of γ in terms of a_0

$$\gamma \simeq \sqrt{1+a_0^2} = \sqrt{1+\frac{I_{18}\lambda_{\mu m}^2}{1.37}} \tag{1.32}$$

where I_{18} is the peak intensity of the laser pulse in $1\times10^{18}\,\text{W cm}^{-2}$ and $\lambda_{\mu m}$ is the wavelength in μm. In 1992, Wilks[2] conducted simulations to show that T_h is on the order of U_p.

$$k_B T_h = mc^2(\gamma-1) \tag{1.33}$$

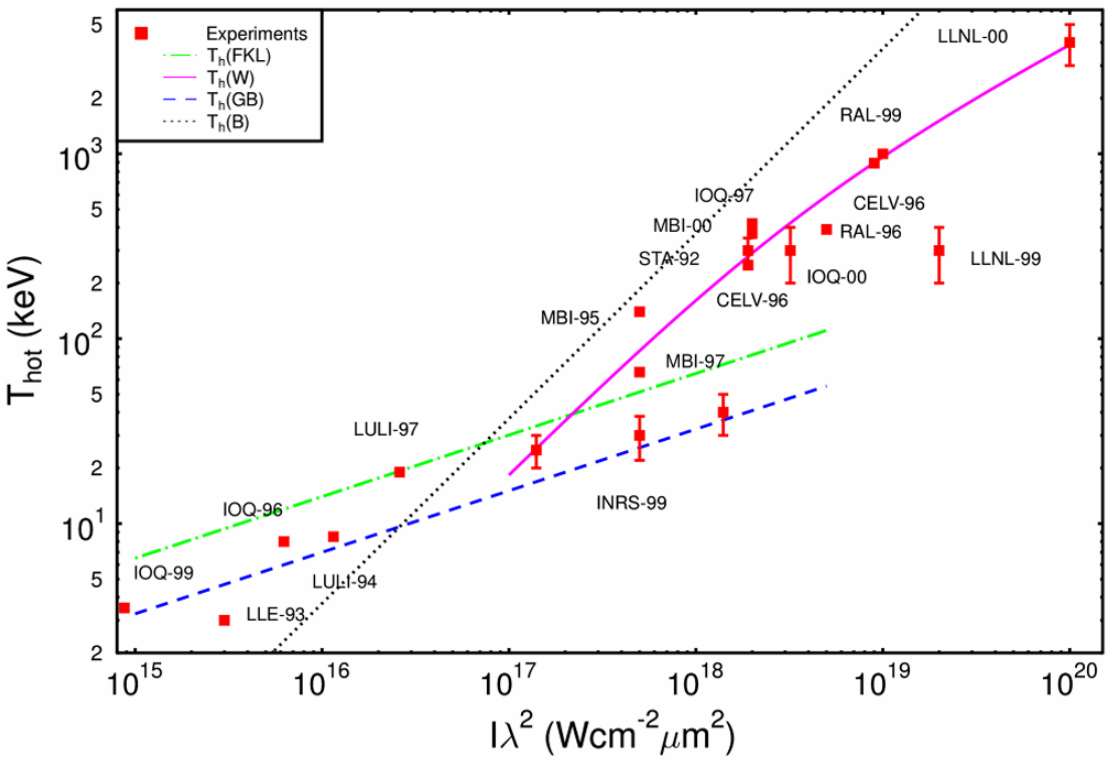

Figure 1.4: Experimentally recorded hot electron temperatures as a function of irradiance $I\lambda^2$ are plotted as red squares. The empirical scaling models are given by Wilks[2](pink, solid), Gibbon and Bell[3](blue, ashed), Forslund et. al.[4](green, dash-dot), and Brunel[5](black, dotted). Figure is taken from Gibbon[6]

In fig. 1.4, we can see that the *Wilks scaling* (pink) closely matches ultra-intense laser experiments. The other scalings in the figure are similarly validated by computational simulations and are all proportional to $(I\lambda^2)^\alpha$, where $0 < \alpha \leq 1$. As a result, the product $I\lambda^2$ is an important quantity in laser-plasma experiments and is called the *irradiance*.

Wilks also outlines a way to measure the hot electron temperature in his simulations[2] by taking the slope of $\frac{dN_e}{dE}$ in the MeV regime and is something I do in (CITE DUB PULSE SIM FIGUR HOT ELECTRON)

Since protons are 1836 times as massive as electrons, they are much harder to accelerate and on the scale of femtosecond pulse interactions, they are essentially immobile. (CITATION) Despite this, ultra-intense laser experiments have demonstrated proton acceleration is possible. This section will explain the Target Normal Sheath Acceleration (TNSA) mechanism for accelerating protons and light ions which is heavily dependent on T_h. Then, we will discuss alternative acceleration mechanisms. Finally, we'll overview some important applications.

1.2.1 Target Normal Sheath Acceleration

The observation of energetic protons off the rear side of thin plastic and gold targets has been documented throughout a variety of experiments since the 80s[22]. It might sound unintuitive that we would even see protons in the first place; after all, when shooting a target like aluminum, one would expect aluminum ions. It turns out that there is always an important and measurable surface contamination layer, primarily composed of hydrogen and light hydrocarbons[23]. Allen [24] showed that when removing the surface contaminant from the backside, we see a strong suppression in ion acceleration. This points to the contaminant layer being the crux of what is accelerated.

TNSA Models

Expansion models have been long known since the 70s and 80s (e.g. Crowe[25] and Kishimoto[26]) that describe the acceleration of protons with experiments (e.g. Tan[22]) as well. However, the advent of Chirped Pulse Amplification[27] in 1985 by Donna Strickland and Gerard Mourou allowed the intensities of the laser light to increase to relativistic levels ($a_0 > 1$) with sub-ps pulse durations. This technology dramatically impacted the field of laser-plasma interactions because it allowed new relativistic regimes of ion acceleration to be explored – for this work they won the Nobel Prize[28].

The field of ultra-intense proton acceleration kicked off in the year of 2000 with a group at Michigan[29] finding 1.6 MeV protons from a thin aluminum foil with a $3 \times 10^{18}\,\mathrm{W\,cm^{-2}}$ class laser at normal incidence. Then, Rutherford Appleton Laboratory found 30 MeV protons[30] from a $5 \times 10^{19}\,\mathrm{W\,cm^{-2}}$ class laser incident on a lead target at 45° incidence. Shortly after, LLNL found energies up to 58MeV[31] from a $3 \times 10^{20}\,\mathrm{W\,cm^{-2}}$ class laser on a gold target at 45° incidence.

Now that efficient MeV proton acceleration had been achieved through multiple studies, a more thorough comprehensive picture of the physical process was desired. In 2001, Wilks[32] summarized much of the existing literature including isothermal expansion model[25], existence of a maximum cutoff energy[26], and dependence on hot temperature [2]. Then, he described the Target Normal Sheath Acceleration process in the following way[32]

> ... the prepulse creates large plasma in front of a solid target. Once the main pulse hits the target, a cloud of energetic electrons (1-10 MeV in effective temperature) is generated, which extends past the ions on both the front and back of the target. Since the protons on the back are in a sharp, flat density gradient, they are accelerated quickly (in the first few μm off the target) to high energies in the forward direction ... On the front, the outermost ions are in a sphere, in a long scale length plasma (due to prepulse) and therefore are accelerated to lower energies are spread out into 2π steradians.

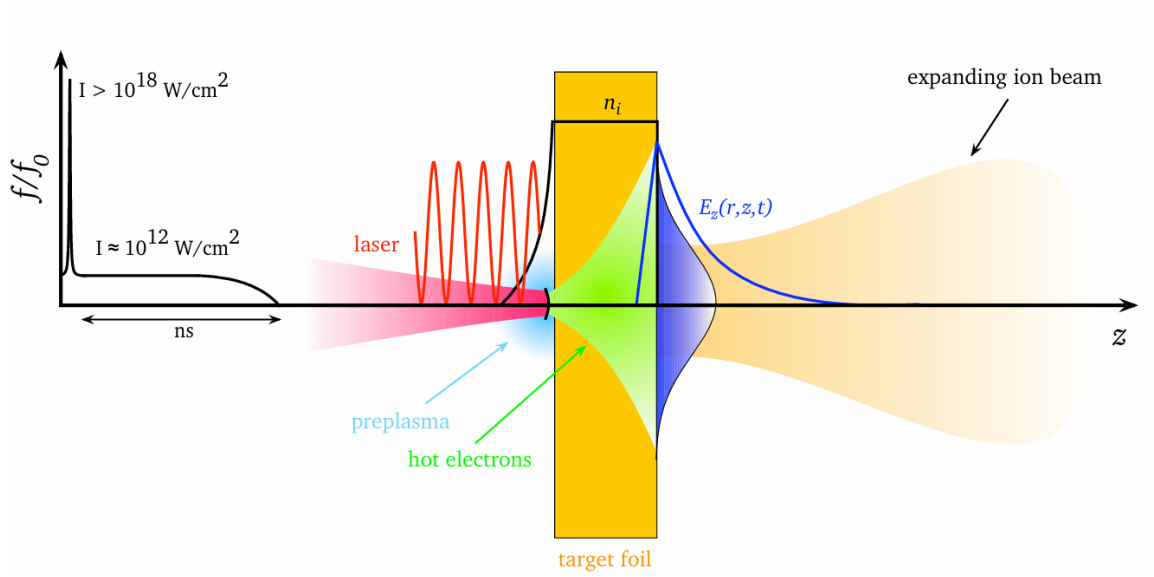

Figure 1.5: The Target Normal Sheath Acceleration (TNSA) process is depicted. First, an intense laser pulse irradiates the front side of a target foil of few μm thickness. This generates hot electrons that stream through the foil and re-emerge in a cloud on the rear side. The charge separation of the hot electrons and positively charged target creates intense longitudinal fields ($\sim$ TV/m) that accelerate light ions in the mostly target normal direction. This figure was taken from Roth[7]

A visual of the TNSA process can be seen in fig. 1.5. Although Wilks[32] provided a physical picture of the TNSA process, existing models didn't always match up to experiments. For this reason, the ensuing decade saw much progress in the development of models to describe the spectrum of TNSA accelerated protons. Perego[33] gives a good review of some of the leading models developed and tested against experiments in the 2000s and these models will be summarized below.

First, are the isothermal expansion (fluid) models which include Mora's "Plasma Expansion into a Vacuum"[34] (2003) which combines eqs. (1.4) and (1.20) with fluid **????**. This model underlies the work done in **??**, where it is explained in more detail, and has the issue of predicting proton energies that can go up to arbitrarily high values. As a remedy, Mora introduces a finite acceleration time τ which is of the order of the pulse duration. Mora[35] addresses this in a different way (2005) by instead assuming an adiabatic model and limiting the target to be a thin foil (instead of a semi-infinite target).

Alternatively, Passoni and Lontano[36] introduces an upper limit to the integration range of the electric potential instead of using the fluid equations. In this approach, the electrostatic fields determined from the potential are considered static, and the ensuing ion dynamics is determined by placing a test ion in the field. Further iterations incorporate

some distribution of speeds for the electrons (non-relativistic Maxwell-Boltzmann[37] or relativistic Maxwell-Juttner[38]) and use an empirically determined scaling for the peak energy of electrons (as a function of laser energy) that do not escape the system[39].

Furthermore, some hybrid models include elements of both fluid and quasistatic models like Robinson[40] and Albright[41].

Optimization of TNSA process

Since the TNSA process is intimately related to the hot electron process at the front of the target and the flat density gradient at the back, many efforts have been taken to design targets that optimize ion acceleration. Patel[42] used spherically shaped targets to act as a lens that can focused the proton beam. MacKinnon[43] showed lower target thickness leads to higher proton energy due to a higher mean density of hot electrons at the surface. More recent experiments have even used nanowires[44] and microtubes[45]. Many experiments generally find that there is an optimal level of pre-expansion of the target that enhances hot electron generation and ion acceleration (e.g. McKenna[46]).

Another way to increase the peak proton energy of the emitted spectrum is to use two spatially aligned pulses. If one pulse has a delay with respect to the other, the first pulse could pre-expand the target to provide an optimal electron density at the front surface[47]. If the pulses are also temporally aligned, the constructive interfere at the target front surface may prove beneficial[48]. The second approach is called *Enhanced Target Normal Sheath Acceleration* (eTNSA) and chapter 2 is devoted to this phenomenon.

See the review article by Roth[7] for a more comprehensive list of the different approaches to enhance TNSA.

1.2.2 Other Acceleration Mechanisms

TNSA is not the only method in which protons can be accelerated. For intensities of greater than 10^{21} W cm^{-2}, laser-induced ion shocks can start to play a significant role[49]. For even higher intensities $\sim 10^{23}$ W cm^{-2}, the radiation pressure of the electromagnetic wave can efficiently transfer momentum to the ions[49]. See Macchi[21] for a more in depth discussion on these topics. One way to differentiate the TNSA regime from other regimes is through the following equation relating a_0 to various properties of the laser and target

$$a_0 = n_e \lambda r_e l_0 = 224 \left(\frac{n_e}{1 \times 10^{29}\,\mathrm{m}^{-3}} \right) \left(\frac{l_0}{1\,\mu\mathrm{m}} \right) \tag{1.34}$$

Lezhnin[8] uses this equation to differentiate TNSA from two other mechanisms: Radiation Pressure Acceleration (RPA) and Coulomb Explosions; this can be seen in fig. 1.6. If the laser intensity is sufficiently high and density is low enough to be transparent, the laser

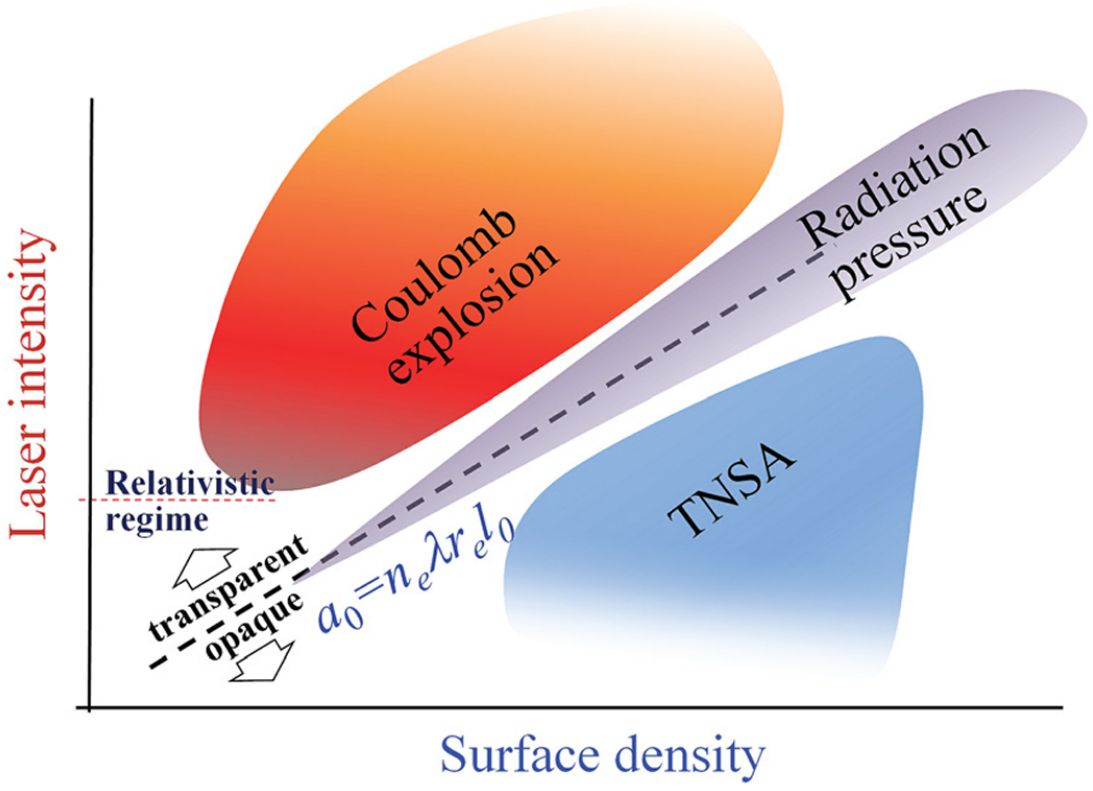

Figure 1.6: The regimes of various three different acceleration mechanisms are displayed in terms eq. (1.34). This figure was taken from Roth[8]

can quickly sweep away most electrons to leave a strongly positive target left behind. The repelling coulomb force will cause the protons to expand outwards in all directions.

When the radiation pressure $P_{\text{rad}} \approx 2I_0/c$ is significant enough to overcome the thermal expanding pressure $n_e k_B T_e$, ions can accelerate directly through the transfer of momentum.[21]. In this regime, laser absorption into hot electrons by traditional mechanisms would be detrimental. By shooting the laser at normal incidence with circular polarization, resonance absorption and $\vec{J} \times \vec{B}$ heating can be minimized as seen in section 1.1.4.

For thick targets, this immense pressure can impart a parabolic deformation that allows the laser to penetrate further. This is the regime of *hole boring*. Targets thin enough where the hole boring process reaches the target rear in a time less than the pulse duration are in the *light sail* regime.

Wakefield Acceleration

All the aformentioned acceleration processes only make sense for overdense targets whose electron density is greater than the critical density ($n_e > n_c$). This is because the critical density surface is the primary area where the laser deposits energy into hot electrons. If the target plasma has $n_e < n_c$, the target is said to be underdense and there is no critical density surface where the laser interacts with. Tajima and Dawson[50] first proposed the idea of a "Laser Electron Accelerator" in 1979 that is capable of accelerating electrons to high energies through the non-linear ponderomotive force. If the conditions are just right, the electrons can "surf" a plasma wave in the wake of the pulse and pull along positive ions in a process now known as *Laser Wakefield Acceleration*. A comprehensive review of the subject can be found in this review[51].

1.2.3 Notes

should talk about Bragg Peak and how that works based on coulomb collision

E = kT / e L where L is related to the debye length or scale length

Heavy ions stay still, hot electrons expand out several debye lengths: causes charge separation that accelerates light ions/protons. Characteristic: accelerated in the normal direction even though laser is at oblique incidence. High scale reduces TNSA electric field b/c boundaries are not as sharp on the backside (to make a capacitor like field).

Spectrum of TNSA beams is typically broadband up to a cutoff energy. The dN/dE looks kind of thermal i.e. exponentially decaying.

Also, a sharp angular boundary in the proton angular distribution (clearer in higher Z and thicker targets) is consistent with a bell-shaped transverse distribution of hot electrons in the rear surface sheath due to the fact that the density will naturally be higher along the laser axis and decreases with transverse radius.

Then, they talk about TNSA modeling which I've already covered: Passoni, Mora, etc.

Can look at Joe Smith's TNSA experiment paper (is it on arxiv?) to see better evidence of the relationships and how they fare with experiments.

Can give a simple estimate of the regime it is relevant by considering intensities where we get relativistic ions. However, this is really, really high and thus why we consider TNSA as the dominant mechanism. We don't have lasers this high of an intensity for these affects to be relevant, so it must come from TNSA i.e. strong electrostatic fields from electrons rather than direct electron acceleration.

Then, in the relativistic transparency regime of thin targets, the laser pulse can actually deposit well into the target. Of course, this means that the laser isn't pushing on the front edge of the target so that we aren't in the RPA regime anymore. In this regime, the Breakout afterburner (BOA) model is typically employed.

Finally collisionless shock acceleration (CSA) becomes relevant when shocks appear and ions reflect off this shock front with speed $2v_s$ where $v_s = Mc_s$ and $M > 1$ is the Mach number. [52] talks about how shock acceleration is optimal for near critical density targets that particularly have an exponential scale length plasma on the rear side of $L_g \approx \lambda_0/2\sqrt{m_i/m_e}$ for uniform electron heating and ion reflection. They also say that the target should be thin enough so that $L < 2\pi c/\omega_{p,i}$ but not too much smaller.

Chapter 2

Particle-in-Cell Simulations of Enhanced Target Normal Sheath Acceleration

This chapter details the work I did in conducting PIC simulations to better understand the Enhanced Target Normal Sheath Acceleration (eTNSA) mechanism that our group tried to demonstrate using LLNL's Titan Laser in March of 2024. As a result, I will mostly focus on the simulation aspect, but include some relevant comparisons to the experiment.

2.1 Theory

2.1.1 Prior Work

[53] first investigated experimentally using two pulses to enhance laser proton acceleration. These pulses had a temporal separation of 0.75-2.5ps and the idea behind it was that the partial pre-expansion of the target from the first pulse (of lesser energy) would enhance the laser absorption (McKenna Laser Part Beams 26 591 2008). This is offset by expansion in the rear surface (Fuchs et al PRL 99 015002 2007 or Borghesi PRL 92 055003 2004).

Scott 2012 APL 101 discovered a similar enhancement using a target that is composed of a foil with a half circle to help reflect the fields back into the foil and increase absorption.

Explain what contrast is: peak of the laser pulse compared to the pedestal and maybe give a diagram.

[47] talks about how colliding two pulses with different levels of temporal delay can enhance proton acceleration. He finds that ultimately, 0 or a small delay is optimal and as the delay gets larger and larger, the enhancement just turns into single pulse. He finds acceleration process can be affected by the second pulse for time delays as long as 0.6ps for 3 micron targets and 1 ps for 6 micron targets. Since we're looking at a 15 micron target, I'd imagine this time would be around 2ps, but I could solve his equations to get a better estimate. This time coincides when the fastest ions have moved a distance of the order of

the transverse extent of the electric sheath field.

[48] talks about how prior studies have attempted to increase proton energy by using two pulses. Whether explicitly (Markey) or through structured targets that reflect the pulse (Scott). The problem is that these approaches involve exploiting the delicate balance between plasma expansion on the front side (increasing absorption in electrons) and rear surface expansion (decreasing effectiveness of TNSA process which relies on non expanded rear). The double pulse approach enhances electric fields and hot electron generation process. They show 45 degrees is the optimal angle for single pulse, but lower angles fare much worse. For double pulse, angles are more resilient. AND a big difference is that the two pulses now have opposite incidence angles which is important because the pulses can now interfere with the reflections and produce a standing wave pattern at the front side of the target.

Explain RCF stacks

2.2 Simulations

2.3 Discussion

Bibliography

[1] Joseph Richard Harrison Smith. *Advanced Simulations and Optimization of Intense Laser Interactions*. PhD thesis, The Ohio State University, May 2020. Available at http://rave.ohiolink.edu/etdc/view?acc_num=osu1589302684037632.

[2] S. C. Wilks, W. L. Kruer, M. Tabak, and A. B. Langdon. Absorption of ultra-intense laser pulses. *Phys. Rev. Lett.*, 69:1383–1386, Aug 1992.

[3] Paul Gibbon and A. R. Bell. Collisionless absorption in sharp-edged plasmas. *Phys. Rev. Lett.*, 68:1535–1538, Mar 1992.

[4] D. W. Forslund, J. M. Kindel, and K. Lee. Theory of hot-electron spectra at high laser intensity. *Phys. Rev. Lett.*, 39:284–288, Aug 1977.

[5] F. Brunel. Not-so-resonant, resonant absorption. *Phys. Rev. Lett.*, 59:52–55, Jul 1987.

[6] Paul Gibbon. *Short Pulse Laser Interactions with Matter*. Imperial College Press, 2005.

[7] M. Roth and M. S. Schollmeier. Ion acceleration - target normal sheath acceleration. In *Proceedings of the 2014 CAS-CERN Accelerator School: Plasma Wake Acceleration*, volume 1, pages 231–270, 2 2016.

[8] K. V. Lezhnin, F. F. Kamenets, V. S. Beskin, M. Kando, T. Zh. Esirkepov, and S. V. Bulanov. Effect of electromagnetic pulse transverse inhomogeneity on ion acceleration by radiation pressure. *Physics of Plasmas*, 22(3):033112, 03 2015.

[9] F.F. Chen. *Introduction to Plasma Physics and Controlled Fusion*. Springer, 3 edition, 2015.

[10] Andrew Zangwill. *Modern Electrodynamics*. Cambridge University Press, 2012.

[11] Andrea Macchi. *A Superintense Laser-Plasma Interaction Theory Primer*. Springer, 2013.

[12] William Kruer. *The Physics of Laser Plasma Interactions*. CRC Press, 2003.

[13] N. G. Denisov. On a singularity of the field of an electromagnetic wave propagated in an inhomogeneous plasma. *Soviet Physics JETP*, 4(4):544–553, 5 1957.

[14] D. W. Forslund, J. M. Kindel, Kenneth Lee, E. L. Lindman, and R. L. Morse. Theory and simulation of resonant absorption in a hot plasma. *Phys. Rev. A*, 11:679–683, Feb 1975.

[15] J. P. Freidberg, R. W. Mitchell, R. L. Morse, and L. I. Rudsinski. Resonant absorption of laser light by plasma targets. *Phys. Rev. Lett.*, 28:795–799, Mar 1972.

[16] K. G. Estabrook, E. J. Valeo, and W. L. Kruer. Two-dimensional relativistic simulations of resonance absorption. *The Physics of Fluids*, 18(9):1151–1159, 09 1975.

[17] P. B. Corkum. Plasma perspective on strong field multiphoton ionization. *Phys. Rev. Lett.*, 71:1994–1997, Sep 1993.

[18] NobelPrize.org. Press release, 2023.

[19] David J. Griffiths. *Introduction to Electrodynamics*. Cambridge University Press, 4 edition, 2017.

[20] W. L. Kruer and Kent Estabrook. J×b heating by very intense laser light. *The Physics of Fluids*, 28(1):430–432, 01 1985.

[21] A. Macchi, M. Borghesi, and M. Passoni. Ion acceleration by superintense laser-plasma interaction. *Rev. Mod. Phys.*, 85:751–793, May 2013.

[22] T. H. Tan, G. H. McCall, and A. H. Williams. Determination of laser intensity and hot-electron temperature from fastest ion velocity measurement on laser-produced plasma. *The Physics of Fluids*, 27(1):296–301, 01 1984.

[23] S. J. Gitomer, R. D. Jones, F. Begay, A. W. Ehler, J. F. Kephart, and R. Kristal. Fast ions and hot electrons in the laser–plasma interaction. *The Physics of Fluids*, 29(8):2679–2688, 08 1986.

[24] M. Allen, P. K. Patel, A. Mackinnon, D. Price, S. Wilks, and E. Morse. Direct experimental evidence of back-surface ion acceleration from laser-irradiated gold foils. *Phys. Rev. Lett.*, 93:265004, Dec 2004.

[25] J. E. Crow, P. L. Auer, and J. E. Allen. The expansion of a plasma into a vacuum. *Journal of Plasma Physics*, 14(1):65–76, 1975.

[26] Yasuaki Kishimoto, Kunioki Mima, Tsuguhiro Watanabe, and Kyoji Nishikawa. Analysis of fast-ion velocity distributions in laser plasmas with a truncated Maxwellian velocity distribution of hot electrons. *The Physics of Fluids*, 26(8):2308–2315, 08 1983.

[27] Donna Strickland and Gerard Mourou. Compression of amplified chirped optical pulses. *Optics Communications*, 56(3):219–221, 1985.

[28] NobelPrize.org. Press release, 2018.

[29] A. Maksimchuk, S. Gu, K. Flippo, D. Umstadter, and V. Yu. Bychenkov. Forward ion acceleration in thin films driven by a high-intensity laser. *Phys. Rev. Lett.*, 84:4108–4111, May 2000.

[30] E. L. Clark, K. Krushelnick, M. Zepf, F. N. Beg, M. Tatarakis, A. Machacek, M. I. K. Santala, I. Watts, P. A. Norreys, and A. E. Dangor. Energetic heavy-ion and proton generation from ultraintense laser-plasma interactions with solids. *Phys. Rev. Lett.*, 85:1654–1657, Aug 2000.

[31] R. A. Snavely, M. H. Key, S. P. Hatchett, T. E. Cowan, M. Roth, T. W. Phillips, M. A. Stoyer, E. A. Henry, T. C. Sangster, M. S. Singh, S. C. Wilks, A. MacKinnon, A. Offenberger, D. M. Pennington, K. Yasuike, A. B. Langdon, B. F. Lasinski, J. Johnson, M. D. Perry, and E. M. Campbell. Intense high-energy proton beams from petawatt-laser irradiation of solids. *Phys. Rev. Lett.*, 85:2945–2948, Oct 2000.

[32] S. C. Wilks, A. B. Langdon, T. E. Cowan, M. Roth, M. Singh, S. Hatchett, M. H. Key, D. Pennington, A. MacKinnon, and R. A. Snavely. Energetic proton generation in ultra-intense laser–solid interactions. *Physics of Plasmas*, 8(2):542–549, 02 2001.

[33] C. Perego, A. Zani, D. Batani, and M. Passoni. Extensive comparison among target normal sheath acceleration theoretical models. *Nuclear Instruments and Methods in Physics Research Section A: Accelerators, Spectrometers, Detectors and Associated Equipment*, 653(1):89–93, 2011. Superstrong 2010.

[34] P. Mora. Plasma expansion into a vacuum. *Phys. Rev. Lett.*, 90:185002, May 2003.

[35] P. Mora. Thin-foil expansion into a vacuum. *Phys. Rev. E*, 72:056401, Nov 2005.

[36] M. Passoni and M. Lontano. One-dimensional model of the electrostatic ion acceleration in the ultraintense laser–solid interaction. *Laser and Particle Beams*, 22(2):163–169, 2004.

[37] Maurizio Lontano and Matteo Passoni. Electrostatic field distribution at the sharp interface between high density matter and vacuum. *Physics of Plasmas*, 13(4):042102, 04 2006.

[38] M. Passoni and M. Lontano. Theory of light-ion acceleration driven by a strong charge separation. *Phys. Rev. Lett.*, 101:115001, Sep 2008.

[39] C. Perego, D. Batani, A. Zani, and M. Passoni. Target normal sheath acceleration analytical modeling, comparative study and developmentsa). *Review of Scientific Instruments*, 83(2):02B502, 02 2012.

[40] A. P. L Robinson, A. R. Bell, and R. J. Kingham. Effect of target composition on proton energy spectra in ultraintense laser-solid interactions. *Phys. Rev. Lett.*, 96:035005, Jan 2006.

[41] B. J. Albright, L. Yin, B. M. Hegelich, Kevin J. Bowers, T. J. T. Kwan, and J. C. Fernández. Theory of laser acceleration of light-ion beams from interaction of ultrahigh-intensity lasers with layered targets. *Phys. Rev. Lett.*, 97:115002, Sep 2006.

[42] P. K. Patel, A. J. Mackinnon, M. H. Key, T. E. Cowan, M. E. Foord, M. Allen, D. F. Price, H. Ruhl, P. T. Springer, and R. Stephens. Isochoric heating of solid-density matter with an ultrafast proton beam. *Phys. Rev. Lett.*, 91:125004, Sep 2003.

[43] A. J. Mackinnon, Y. Sentoku, P. K. Patel, D. W. Price, S. Hatchett, M. H. Key, C. Andersen, R. Snavely, and R. R. Freeman. Enhancement of proton acceleration by hot-electron recirculation in thin foils irradiated by ultraintense laser pulses. *Phys. Rev. Lett.*, 88:215006, May 2002.

[44] S. Vallieres. Enhanced laser-driven proton acceleration using nanowire targets. *Scientific Reports*, 11, 1 2021.

[45] Joseph. Strehlow. A laser parameter study on enhancing proton generation from microtube foil targets. *Scientific Reports*, 12, 6 2022.

[46] P. McKenna, D.C. Carroll, O. Lundh, F. Nürnberg, K. Markey, S. Bandyopadhyay, D. Batani, R.G. Evans, R. Jafer, S. Kar, and et al. Effects of front surface plasma expansion on proton acceleration in ultraintense laser irradiation of foil targets. *Laser and Particle Beams*, 26(4):591–596, 2008.

[47] J. Ferri, L. Senje, M. Dalui, K. Svensson, B. Aurand, M. Hansson, A. Persson, O. Lundh, C.-G. Wahlström, L. Gremillet, E. Siminos, T. C. DuBois, L. Yi, J. L. Martins, and T. Fülöp. Proton acceleration by a pair of successive ultraintense femtosecond laser pulses. *Physics of Plasmas*, 25(4):043115, 04 2018.

[48] J. Ferri, E. Siminos, and T. Fülöp. Enhanced target normal sheath acceleration using colliding laser pulses. *Communications Physics*, 2:40, 4 2019.

[49] J. Fuchs, P. Antici, E. D'Humières, E. Lefebvre, M. Borghesi, E. Brambrink, C. Cecchetti, M. Kaluza, V. Malka, M. Manclossi, S. Meyroneinc, P. Mora, J. Schreiber, T. Toncian, H. Pépin, and P. Audebert. Laser-driven proton scaling laws and new paths towards energy increase. *Nature Physics*, 2, 12 2005.

[50] T. Tajima and J. M. Dawson. Laser electron accelerator. *Phys. Rev. Lett.*, 43:267–270, Jul 1979.

[51] E. Esarey, C. B. Schroeder, and W. P. Leemans. Physics of laser-driven plasma-based electron accelerators. *Rev. Mod. Phys.*, 81:1229–1285, Aug 2009.

[52] F. Fiuza, A. Stockem, E. Boella, R. A. Fonseca, L. O. Silva, D. Haberberger, S. Tochitsky, W. B. Mori, and C. Joshi. Ion acceleration from laser-driven electrostatic shocksa). *Physics of Plasmas*, 20(5):056304, 04 2013.

[53] K. Markey, P. McKenna, C. M. Brenner, D. C. Carroll, M. M. Günther, K. Harres, S. Kar, K. Lancaster, F. Nürnberg, M. N. Quinn, A. P. L. Robinson, M. Roth, M. Zepf, and D. Neely. Spectral enhancement in the double pulse regime of laser proton acceleration. *Phys. Rev. Lett.*, 105:195008, Nov 2010.